17th Brazilian Congress of Thermal Sciences and Engineering
November 25th-28th, 2018, Águas de Lindóia, SP, Brazil

ENCIT-2018-0061
NUMERICAL STUDY OF A SOLAR LITHIUM BROMIDE-WATER ABSORPTION COOLING SYSTEM

Raquel Miguez Carvalho
Kamal Abdel Radi Ismail
University of Campinas, Faculty of Mechanical Engineering, Department of Energy, Mendeleiev street, 200, Cidade Universitária "Zeferino Vaz", Barão Geraldo, Postal Code 13083.860, Campinas (SP), Brazil
raquel.miguezcarvalho@gmail.com
kamal@fem.unicamp.br

Abstract. *Air conditioners and electric showers are responsible for a large percentage of the daily electricity end-uses in the residential sector in Brazil. These energy demands can be supplied by available solar energy technologies. The objective of this paper is to calculate the cooling load and the overall performance of a solar lithium bromide-water single-effect absorption cooling system powered by a parabolic trough collector (PTC) for residential air conditioning application. The weather input data used are from Campinas-SP, Brazil. Firstly, a home-built numerical code was developed using finite volume method (FVM) to calculate the heat absorbed by the collector and its performance, then the Engineering Equation Solver (EES) software was used to calculate the absorption cooling subsystem performance and its cooling load. The integration of the cooling system with the collector resulted in an overall efficiency of about 50%. The results showed that in summer, the collector capacity of cooling per collector aperture area is 279 BTU/m² for a 24h/day operation and 676 BTU/m² for a 10h/day operation, while in winter, the corresponding values are 205 BTU/m² for a 24h/day operation and 519 BTU/m² for a 10h/day operation.*

Keywords: *solar absorption system, solar energy, cooling cycle, parabolic trough collector, thermal comfort*

1. INTRODUCTION

The air conditioning represents 2-18% of the daily electricity end-uses in the residential sector of the bioclimatic zone of Campinas over summer and 1% in winter, and the electric shower represents 14-28% in summer and 26% over winter (Ghisi et al., 2007). The vapor compression-based refrigeration systems generally employed in air-conditioning operate with synthetic refrigerants and electric energy. Furthermore, approximately 64% of the Brazilian electricity is generated from hydroelectric plants (ANEEL, 2017) that cause irreversible environmental impacts due to inundation of native forests and interfering with the ecosystem. This reinforces the importance of the development of new technologies more environmentally friendly systems and explains the increase of interest in this field.

A solar refrigeration system can be powered by photovoltaic models or thermal collectors. The photovoltaic system firstly converts the incident radiation in electric energy, and then supplies the refrigeration systems. While the solar thermal system supplies thermal energy directly, this makes this second system more efficient. Tzivanidis et al. (2015) developed a small PTC model using Solidworks and conducted simulations for different operating conditions to predict the efficiency of this model and analyze the heat transfer phenomena. Sintali et al. (2014) reported the development of energy equations to calculate the performance of a PTC using solar coordinates including the heat transfer between the components.

A good alternative to replace classical refrigeration systems are the sorption refrigeration systems that can be powered by renewable energy sources (Sarbu; Sebarchievici, 2015). Kim and Ferreira (2008) compared the available solar refrigeration options from an economic and energy efficiency points of view and concluded that a single-effect absorption system powered by solar thermal collectors appears to be the best option.

Aman et al. (2014) developed a thermodynamic model based on a 10 kW air cooled ammonia/water absorption chiller powered by solar thermal energy. They presented the energy and exergy analyses to evaluate the performance of this residential scale cooling system. The COP of their system was 0.60 and the exergetic efficiency was 32.01%. Marc et al. (2015) presented a dynamic model and an experimental validation of a single-effect LiBr/H2O absorption chiller also powered by solar collector operating without any backup system. The COP was calculated for different refrigerating capacity and indicated results between 0.58 for 10 kW and 0.74 for 30 kW.

The solar powered air conditioning still has low values of COP when compared to vapor compression cycles and a high initial cost, mostly because of the collectors. Abu-Zour and Riffat (2007) suggested combining both cooling cycles to reduce CO_2 emissions and save energy.

The solar energy is not the only source that powered a sorption refrigeration system. Benedetti (2010) presents a technical and economic analysis of an ammonia-water absorption system powered by thermal energy from biogas

obtained from by-products from a poultry slaughterhouse to partially replacing a vapor compression system.

This paper presents the thermal and fluid-dynamic simulation of a PTC. The governing equations (continuity, momentum, and energy) were discretized using the FVM and the velocity, pressure and temperature fields are calculated using the SIMPLE algorithm. The numerical model has been validated with experimental data obtained by Sandia National Laboratories for solar a LS-2 module with Cermet selective coating, vacuumed annulus and Syltherm 800 as a working fluid. Three different computational grids were tested. This collector was simulated for the weather data from Campinas-SP, Brazil, for February as a summer month and for June as a winter month. The absorption cooling subsystem equations were solved using EES software for two different operation periods. The predicted performance of the solar collector, cooling load, cooling subsystem performance and system overall performance are presented and discussed.

2. METHODOLOGY

The solar absorption cooling system used in this work and its components are shown in Fig. 1.

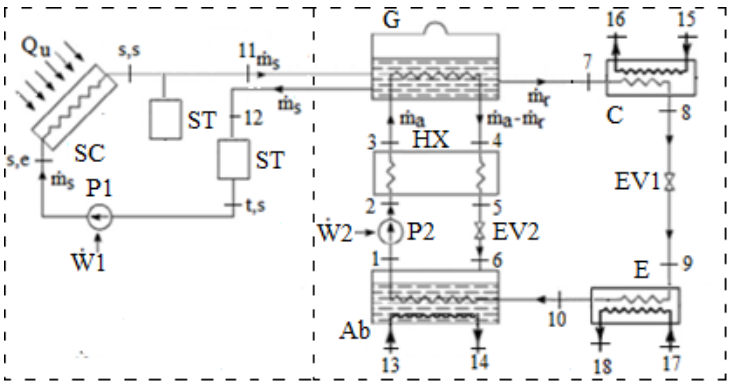

Figure 1. Solar single-effect absorption system. Adapted from Sarbu e Sebarchievici (2015)

To calculate the collector, cooling cycle and overall performance and the cooling load, the system is divided in two parts. The first part is the collector subsystem, it includes the solar collectors (SC), the storage tanks (ST) and a pump (P1) and the second part is the absorption cooling subsystem, it includes the generator (G), the heat exchanger (HX), a pump (P2), two expansion valves (VE1 and VE2), the absorber (Ab), the condenser (C) and the evaporator (E). The storage tanks are important for the present study but will not be presented in details in this paper.

2.1 Collector subsystem

The storage tank is included in the system to ensure continuous operation and reliability of the system, but it is not studied in details in this work. Its loss is considered 5%.

The energy balance on the pump can be written as:

$$\dot{W}_1 = \dot{m}_s \left(h_{sc,in} - h_{st,out} \right) = \frac{P_{sc,in} - P_{st,out}}{\rho} \dot{m}_s \tag{1}$$

Where $\dot{W}_1$ is the work of the pump, $h_{st,out}$ is the outlet enthalpy of the storage tank, $h_{sc,in}$ is the inlet enthalpy of the solar collector, $P_{sc,in}$ is the inlet pressure of the collector, $P_{st,out}$ is the outlet pressure of the storage tank and ρ is the density of the working fluid.

The collector studied in this work is a PTC with an evacuated tube. It is composed of a receiver and a concentrator. The receiver is where the radiation is absorbed and it is composed of a glass cover, a vacuumed annulus, an absorber and a working fluid. The concentrator is the optical system, it redirects the incident beam radiation from the sun falling on the reflective surface to the receiver surface. Figure 2 shows the PTC and its components.

In order to calculate the amount of heat absorbed by the collector, a numerical code was developed. It uses the FVM to discretize the governing differential equations and the SIMPLE algorithm (Patankar, 1980) to calculate the flow field, pressure field and the variation of temperature in a two-dimensional grid. The variation in angular axis is not considered so that the outlet temperature is the average mixed outlet temperature.

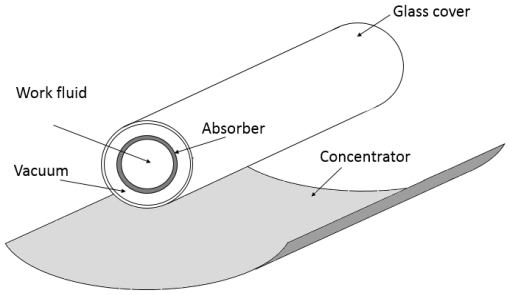

Figure 2. Parabolic trough collector

The governing equations are:

$$\frac{\partial u}{\partial x}+\frac{\partial v}{\partial r}=0 \tag{2}$$

$$\rho u\frac{\partial u}{\partial x}+\rho v\frac{\partial u}{\partial r}=\mu\left(\frac{\partial^2 u}{\partial x^2}+\frac{1}{r}\frac{\partial}{\partial r}\left(r\frac{\partial u}{\partial r}\right)\right)-\frac{\partial p}{\partial x} \tag{3}$$

$$\rho u\frac{\partial v}{\partial x}+\rho v\frac{\partial v}{\partial r}=\mu\left(\frac{\partial^2 v}{\partial x^2}-\frac{v}{r^2}+\frac{1}{r}\frac{\partial}{\partial r}\left(r\frac{\partial v}{\partial r}\right)\right)-\frac{\partial p}{\partial r} \tag{4}$$

$$\rho\left(u\frac{\partial T}{\partial x}+v\frac{\partial T}{\partial r}\right)=\frac{\partial}{\partial x}\left(\frac{k}{c_p}\frac{\partial T}{\partial x}\right)+\frac{1}{r}\frac{\partial}{\partial r}\left(r\frac{k}{c_p}\frac{\partial T}{\partial r}\right)+S \tag{5}$$

There is no flow in the cover, vacuum and the absorber, to ensure zero speed in these components the viscosity was adopted as 10^{35}. The boundary conditions for the energy equation include the solar beam radiation, the air free convection, the radiation exchange between the components and between the glass cover and the sky, the east and west boundary are considered adiabatic and the south of the domain is the axis of symmetry. The boundary conditions are treated in the adjacent control volume internal node as an additional source term and they are:

For all components:

West:

$$\left.\frac{\partial T}{\partial x}\right|_{x=0}=0 \tag{6}$$

East:

$$\left.\frac{\partial T}{\partial x}\right|_{x=L}=0 \tag{7}$$

For the glass cover:

North:

$$\left.k\frac{\partial T}{\partial r}\right|_{r=R\,cover,ext}=\alpha_{cover}q''_{rad,total}+h\left(T\left(x,R_{cover,ext}\right)-T_{air}\right)+\sigma\varepsilon\left(T^4_{cover}\left(x,R_{cover,ext}\right)-T^4_{sky}\right) \tag{8}$$

South:

$$\left.k\frac{\partial T}{\partial r}\right|_{r=R\,cover,\mathrm{int}}=\frac{A_{abs}\sigma\left(\overline{T}^4_{abs}-\overline{T}^4_{cover}\right)}{\frac{1}{\varepsilon_{abs}}+\frac{1-\varepsilon_{cover}}{\varepsilon_{cover}}\left(\frac{R_{abs,ext}}{R_{cover,\mathrm{int}}}\right)} \tag{9}$$

For the absorber:
North:

$$k\frac{\partial T}{\partial r}\bigg|_{r=Rabs,ext} = -\frac{A_{abs}\sigma\left(\overline{T}_{abs}^{4} - \overline{T}_{cover}^{4}\right)}{\frac{1}{\varepsilon_{abs}} + \frac{1-\varepsilon_{cover}}{\varepsilon_{cover}}\left(\frac{R_{abs,ext}}{R_{cover,int}}\right)} + \tau_{cover}\alpha_{abs}q''_{rad,total} \tag{10}$$

For the work fluid:
South:

$$k\frac{\partial T}{\partial r}\bigg|_{r=0} = 0 \tag{11}$$

The boundary conditions of the momentum equations for the working fluid are:
North:

$$u(x,R_{f,ext}) = 0 \tag{12}$$

$$v(x,R_{f,ext}) = 0 \tag{13}$$

South:

$$v(x,0) = 0 \tag{14}$$

$$\frac{\partial u}{\partial x}\bigg|_{r=0} = 0 \tag{15}$$

West:

$$u(0,r) = u_{in} \tag{16}$$

$$v(0,r) = 0 \tag{17}$$

East:

$$\frac{\partial u}{\partial x}\bigg|_{x=L} = 0 \tag{18}$$

$$\frac{\partial v}{\partial r}\bigg|_{x=L} = 0 \tag{19}$$

The thermal efficiency is calculated as:

$$\eta_t = \frac{\dot{m}_f cp_f\left(T_{f,out} - T_{f,in}\right)}{q''_{rad,total}\,A} \tag{20}$$

The system is considered to be installed in Campinas-SP, Brazil, located in latitude 22°54'S. The global horizontal irradiance (GHI) available in the SWERA website has been converted in the direct normal irradiance (DNI) incident in the aperture plane of the collector using the equations in Duffie and Beckman (2013) for a collector with the horizontal single axis tracker system. This is needed because the concentrator only redirects the beam radiation. The geometrical concentration of this kind of collector is calculated as (Duffie; Beckman, 2013):

$$GC = \frac{Y}{\pi D} \tag{21}$$

Where Y is the width of the concentrator and D is the diameter of the absorber.
The concentrator has an optical performance calculated according to (Zarza Moya; Ciemat, 2012):

$$\eta_{opt,\theta\neq 0^\circ} = \eta_{opt,\theta=0^\circ} K(\theta) \tag{22}$$

Where $K(\theta)$ is the incidence angle modifier and it is calculated as (Zarza Moya; Ciemat, 2012):
For ($0° < \theta < 80°$):

$$K(\theta) = 1 - 2.23073\times10^{-4}\theta - 1.1\times10^{-4}\theta^2 + 3.18596\times10^{-6}\theta^3 - 4.85509\times10^{-8}\theta^4 \tag{23}$$

For ($85° < \theta < 90°$):

$$K(\theta) = 0 \tag{24}$$

The average natural heat transfer convection is calculated from Eq. (26) and the hourly air temperature is calculated using the maximum and minimum daily temperatures as in ASHRAE (2001). Both wind speed and maximum and minimum temperatures data are available in the Weather Spark website.
The wind speed obtained from Weather Spark is for 10 m height. To calculate the corresponding speed for 2 m height we used the following equation, (Munhoz; Garcia, 2008):

$$\frac{U_1}{U_2} = \left(\frac{z_1}{z_2}\right)^{0.143} \tag{25}$$

Where U_1 is the speed corresponding to the altitude z_1 and U_2 is the speed corresponding to the altitude z_2.
The average Nusselt number for an external flow normal to a cylinder can be calculated as (Incropera et al., 2008):

$$\overline{Nu}_D \equiv \frac{\bar{h}D}{k} = C\,\mathrm{Re}_D^m\,\mathrm{Pr}^{1/3} \tag{26}$$

Where $\bar{h}$ is the average convective heat transfer coefficient, D is the diameter of the glass cover, k is the thermal conductivity, C and m are constants equal to 0.193 and 0.618, respectively, for Reynolds between 4,000 and 40,000 (Incropera et al., 2008), Re_D is the Reynolds number and Pr is the Prandtl number.
Reynolds number is calculated as:

$$\mathrm{Re}_D = \frac{VD}{\nu} \tag{27}$$

Where V is the wind speed and ν is the kinematic viscosity.
The temperature of the sky is calculated as (García-Valladares; Velázquez, 2009):

$$T_{sky} = 0.0552 T_{air}^{1.5} \tag{28}$$

The radiation exchange between the glass cover and the absorber is calculated as (Kreith; Bohn, 2003):

$$q_{abs\leftrightarrow cover} = A_{abs} F_{abs-cover} \sigma\left(\bar{T}_{abs}^4 - \bar{T}_{cover}^4\right) \tag{29}$$

Where $\bar{T}_{abs}$ is the average temperature of the absorber and $\bar{T}_{cover}$ is the average temperature of the cover, $F_{abs\text{-}cover}$ is the form factor and is calculated as:

$$F_{abs-cover} = \frac{1}{\left(1-\varepsilon_{abs}\right)/\varepsilon_{abs} + 1 + A_{abs}\left(1-\varepsilon_{cover}\right)/A_{cover}\varepsilon_{cover}} \tag{30}$$

Where ε_{abs} is the emmitance of the absorber.

2.1.1 Validation and grid test

To ensure that the results will be independent of the grid size, grid size analysis was done. The experimental data from Dudley et al. (1994) for a LS-2 module with Cermet selective coating, vacuumed annulus and Syltherm 800 as a working fluid were selected. The others parameters are shown in Tab. 1 and the experimental data in Tab. 2. The properties of the Syltherm 800 are in the technical data sheet available in the Loikits Distribution website and they change with the local temperature.

Table 1. PTC specifications

Characterization	PTC specification
Length / Width	7.8 m / 5 m
Focal distance	1.84 m
$D_{abs,int}$ / $D_{abs,ext}$	0.066 m / 0.07 m
$D_{cover,int}$ / $D_{cover,ext}$	0.115 m / 0.109 m
Absorber absorptance	0.906
Absorber emittance	0.14
Glass cover emittance	0.08
Reflected surface reflectivity	0.93
Interception factor	0.92

Table 2. Experimental data from Dudley et al. (1994)

Direct Normal Insolation [w/m²]	Flow rate [L/min]	Wind speed [m/s]	Air Temp [K]	Temp In [K]	Temp Out [K]
968.2	47.8	3.7	295.4	424.0	446.3

Three different computational grids were studied. The percentage of difference in outlet temperature from the experimental data was calculated and it is shown in Tab. 3. The relative difference between the experimental values of T_{out} and the predicted value for grid 3 is in good agreement with the experimental data of Dudley et al. (1994) and it can be considered sufficiently accurate. Hence, all simulations for the rest of the study will be conducted using this grid.

Table 3. Grid testing

Grid	Radial nodes	Axial nodes	Total nodes	Tout [K]	Difference with exp ±%
1	19	19	361	446.19	0.0246
2	30	30	900	446.32	0.0045
3	41	41	1681	446.31	0.0022

2.2 Absorption cooling subsystem

The components of the absorption cooling subsystem are treated as “black-boxes” and some considerations are made:

- Negligible pressure losses in the pipes.
- Negligible heat loss to the environment.
- There are no kinetic or potential energy variations.

And the absorption cooling system obeys to the balance of mass, specie and energy in steady state (Benedetti, 2010).

$$\sum_{in} \dot{m}_{in} - \sum_{out} \dot{m}_{out} = 0 \tag{31}$$

$$\sum_{in} \dot{m}_{in} x_{in} - \sum_{out} \dot{m}_{out} x_{out} = 0 \tag{32}$$

$$Q - \dot{W} + \sum_{in} \dot{m}_{in} h_{in} - \sum_{out} \dot{m}_{out} h_{out} = 0 \tag{33}$$

Where $\dot{m}$ is the mass flow rate, x is the mass fraction of the absorbent, Q is heat, $\dot{W}$ is work and h is enthalpy. The equations of this subsystem were separated in two subsections, the absorption subsection and the cooling subsection.

2.2.1 Absorption subsection

This subsection includes the generator, the heat exchanger, a pump, an expansion valve and the absorber. The working fluid of this part is a solution of water and lithium bromide. There are two mass flow rates, the first one, $\dot{m}a$, leaves the absorber and goes to the generator, passing through a pump and the heat exchanger in the left side. The other flow rate, $\dot{m}a$ - $\dot{m}r$, leaves the generator and goes to the absorber passing through the heat exchanger in the right side and an expansion valve, while $\dot{m}r$ is the mass flow rate of refrigerant that leaves the generator to goes to the condenser in the vapor phase.

The specie balance in the generator is:

$$\dot{m}_a x_3 - \left(\dot{m}_a - \dot{m}_r\right) x_4 = 0 \tag{34}$$

The energy balance in the generator is:

$$Q_g = \dot{m}_r h_7 + \left(\dot{m}_a - \dot{m}_r\right) h_4 - \dot{m}_a h_3 \tag{35}$$

Where Q_g is the energy from the collector subsystem:

$$Q_g = \dot{m}_s \left(h_{11} - h_{12}\right) \tag{36}$$

The generator works as a heat exchanger, so the heat can also be calculated as (Herold et al., 1996):

$$Q_g = UA_g \Delta T_{m\lg} \tag{37}$$

Where U is the overall heat transfer coefficient, Ag is the generator heat exchanger surface area, but, in this work UA_g is treated as one variable and $\Delta T_{m\lg}$ is (Herold et al., 1996):

$$\Delta T_{m\lg} = \frac{\left(T_{11} - T_4\right) - \left(T_{12} - T_7\right)}{\ln\left(\frac{T_{11} - T_4}{T_{12} - T_7}\right)} \tag{38}$$

The heat transfer in the heat exchanger is:

$$Q_{HX} = UA_{HX} \Delta T_{mlHX} \tag{39}$$

Where ΔT_{mlHX} is:

$$\Delta T_{mlHX} = \frac{\left(T_4 - T_3\right) - \left(T_5 - T_2\right)}{\ln\left(\frac{T_4 - T_3}{T_5 - T_2}\right)} \tag{40}$$

The heat transfer can also be calculated in both sides by:

$$Q_{HX} = \dot{m}\left(h_{out} - h_{in}\right) \tag{41}$$

The expansion valve is needed to decrease the fluid pressure. It reduces also the temperature, but the enthalpy does not change.

The energy balance of the absorber is:

$$Q_a = \dot{m}_a h_1 - \dot{m}_r h_{10} - \left(\dot{m}_a - \dot{m}_r\right) h_6 \tag{42}$$

The absorber rejects heat to the environment and eventually can be used for heating water for possible use.
The energy balance of the water that receives heat from the absorber is:

$$Q_a = \dot{m}_{13}\left(h_{14} - h_{13}\right) \tag{43}$$

The energy balance of the pump is:

$$\dot{W}_2 = \dot{m}_a\left(h_2 - h_1\right) = \frac{P_g - P_a}{\rho_{solution}}\dot{m}_a \tag{44}$$

2.2.2 Cooling subsection

The last part includes the condenser, the evaporator and an expansion valve. The refrigerant mass flow rate that circulates through this part is $\dot{m}r$.
The rejected energy from condenser is also used to heat water and it is calculated by:

$$Q_c = \dot{m}_r\left(h_8 - h_7\right) \tag{45}$$

The energy balance of the water that receives the heat from the condenser is:

$$Q_c = \dot{m}_{15}\left(h_{16} - h_{15}\right) \tag{46}$$

The condenser also works as a heat exchanger, this means that the heat exchanger equation also applies to this component (Herold, 1996):

$$Q_c = UA_c\Delta T_{mlc} \tag{47}$$

Where ΔT_{mlc} is (Herold, 1996):

$$\Delta T_{mlc} = \frac{\left(T_{15} - T_8\right) - \left(T_{16} - T_8\right)}{\ln\left(\frac{T_{15} - T_8}{T_{16} - T_8}\right)} \tag{48}$$

The expansion valve is needed to decrease the fluid pressure. It reduces also the temperature, but the enthalpy does not change. A fan coil cools the room. The evaporator cools the water that circulates through the fan coil. The removed heat from this water is:

$$Q_e = \dot{m}_r\left(h_{10} - h_9\right) \tag{49}$$

The energy balance of this water is:

$$Q_e = \dot{m}_{17}\left(h_{18} - h_{17}\right) \tag{50}$$

This last component also works as a heat exchanger, so (Herold et al., 1996):

$$Q_e = UA_e\Delta T_{mle} \tag{51}$$

Where ΔT_{mle} (Herold et al., 1996):

$$\Delta T_{mle} = \frac{\left(T_{17} - T_{10}\right) - \left(T_{18} - T_9\right)}{\ln\left(\frac{T_{17} - T_{10}}{T_{18} - T_9}\right)} \tag{52}$$

The performance of the absorption cooling subsystem is (Herold et al., 1996):

$$COP = \frac{Qe}{Qg} \tag{53}$$

The overall performance of the system can be calculated by multiplying the thermal performance of the collector by the *COP*,

$$\eta_{overall} = \eta_t \cdot COP \tag{54}$$

2.2.3 Validation

To solve these equations EES software was used, since it has a library with the thermodynamics properties of the LiBr-water solution. To verify the accuracy of the model, the data from Herold et al. (1996) was simulated, and their numerical results were compared to the present predictions. The input data from Herold et al. (1996) is shown in Tab. 4.

Table 4. Input data

Input description	Value	Input description	Value
ϵ_{TC}	0.64	$\dot{m}_{13}$ [kg/s]	0.28
$\dot{m}_a$ [kg/s]	0.05	T_{15} [°C]	25
UA_a [kW/K]	1.80	$\dot{m}_{15}$ [kg/s]	0.25
UA_c [kW/K]	1.20	T_{11} [°C]	100
UA_g [kW/K]	1.00	$\dot{m}_{11}$ [kg/s]	1.0
UA_e [kW/K]	2.25	T_{17} [°C]	10
T_{13} [°C]	25	$\dot{m}_{17}$ [kg/s]	0.4

The subscripts of the variables from Tab. 4 are shown in Fig. 3.

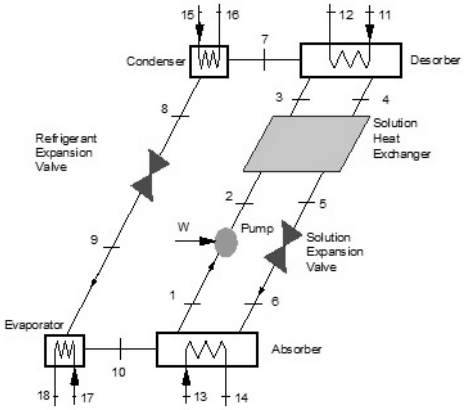

Figure 3. Single-effect absorption cooling system. Source: Herold et al. (1996)

The comparison between the results from Herold et al. (1996) and the present predictions and the percentage differences are shown in Tab. 5. A good agreement has been obtained.

Table 5. Comparison of results

	Herold (numerical)	Present (numerical)	Percentage difference (%)
COP	0.720	0.721 kW	0.139
Qa	14.039 kW	14.040 kW	0.007
Qc	11.213 kW	11.209 kW	0.036
Qg	14.678 kW	14.674 kW	0.027
Qe	10.574 kW	10.575 kW	0.009
W	0.000206 kW	0.000206 kW	0.0

3. RESULTS

3.1 Parabolic trough collector

The LS-2 module with cermet selective coating, vacuumed annulus and Syltherm 800 as a working fluid was simulated for the weather data of Campinas-SP for a summer month, February, and for a winter month, June. The collector aperture area is 39 m². The inlet temperature adopted is 100°C and the outlet temperature is 120°C. The hourly absorbed heat for both months is shown in Tab. 6.

Table 6. Hourly heat absorbed for February and June

Q_{abs} [kW]		
Hour	February	June
6-7h	1.609	0
7-8h	4.590	3.924
8-9h	8.082	6.440
9-10h	11.539	8.972
10-11h	14.319	11.035
11-12h	15.866	12.193
12-13h	15.866	12.194
13-14h	14.319	11.035
14-15h	11.539	8.972
15-16h	8.083	6.439
16-17h	4.590	3.924
17-18h	1.609	0

The thermal losses from the storage tank are adopted as 5% of the daily absorbed heat. The direct normal irradiation, the beam radiation incident on the collector aperture area, the daily absorbed heat, the thermal performance of the collector and the absorbed heat including losses for both months are presented in Tab. 7.

Table 7. Thermal performance of the collector

	February	June
I_b [kW/m²]	3.987	3.030
I_b.A [kW]	155.483	11.815
Q_{abs}/day [kW]	112.010	85.128
η_t [%]	72.040	72.048
Q_{abs}/day [kW] including losses	106.409	80.872

3.2 Solar absorption cooling system

The absorbed heat including losses from the storage tank is used as an input data in the absorption cooling subsystem for a 24h/day operation and a 10h/day operation for both months. The absorbed heat per hour, the COP, the cooling load in kW and in Btu and the rejected heat from the absorber and the condenser for both operation periods for February and June are presented in Tab. 8 and 9, respectively.

Table 8. Results for February

Operation	Q_{abs}/h [kW]	COP	Q_e [kW]	Q_e[Btu]	Q_a+Q_c [kW]
24h/day	4.434	0.72	3.191	10,888	18.371
10h/day	10.641	0.726	7.73	26,375	7.625

Table 9. Results for June

Operation	Q_{abs}/h [kW]	COP	Q_e [kW]	Q_e[Btu]	Q_a+Q_c [kW]
24h/day	3.370	0.697	2.348	8,012	14.019
10h/day	8.087	0.734	5.932	20,240	5.718

The thermal effectiveness of the system can be increased if the rejected heat is used to generate hot water for domestic or commercial use replacing electric showers and small electric boilers. The overall performance for both operation periods and months are shown in Tab. 10.

Table 10. Overall performance

Month	February		June	
Operation	24 h/day	10 h/day	24 h/day	10 h/day
$\eta_{overall}$	51.17%	52.23%	50.21%	52.88%

The overall performance accounts only the cooling load, the heated water is an additional thermal gain. The storage tanks are essential elements without which the system cannot operate adequately especially in cloudy days. A storage tank for the heated water is also needed.

One collector of area of 39 m^2 can replace a 26,000 Btu air conditioner operating 10h per day on summer and a 20,000 Btu on winter. In cold days when air conditioning is not needed, the absorbed heat from the collector can be used directly to produce hot water for domestic and commercial use.

4. CONCLUSIONS

The present study reveals that the collector efficiency is about 72%, the COP is about 0.72 and the integrated cooling system with the collector resulted in an overall efficiency of about 50%. In summer, the collector capacity of cooling per collector aperture area is 279.2 BTU/m² for a 24h/day operation and 676.3 BTU/m² for a 10h/day operation. In winter, it was 205.4 BTU/m² for a 24h/day operation and 519.0 BTU/m² for a 10h/day operation. The above indicators clearly show that the concept is viable and can replace electric energy for this type of applications, reduce greenhouse emissions and preserve the ecosystem.

5. ACKNOWLEDGEMENTS

The authors wish to thank the CNPq for the master scholarship for the first author and for PQ Research Grant for the second author.

6. REFERENCES

Abu-Zour and A.M.; Riffat, S.B., 2007. “Solar-driven air-conditioning cycles: a review”. *The Journal of Engineering Research*, Vol. 4, n. 1, p. 48-63.

Aman, J., Ting, D.S.-K. and Henshaw, P., 2014. “Residential solar air conditioning: Energy and exergy analyses of an ammonia-water absorption cooling system”. *Applied Thermal Engineering*, Vol. 62, p. 424-432.

ANEEL, “Agência Nacional de Energia Elétrica. Capacidade de Geração do Brasil”. 24 Nov. 2017 <http://www2.aneel.gov.br/aplicacoes/capacidadebrasil/capacidadebrasil.cfm>.

ASHRAE, 2001. “ASHRAE Handbook of Fundamentals – Chapter 29: Nonresidential Cooling and Heating Load Calculation Procedures. American Society of Heating, Refrigerating and Air-Conditioning Engineers”. Inc., USA.

Benedetti, T.M., 2010. *Análise técnica e econômica de um sistema de refrigeração por ciclo de absorção amônia-água e sua integração com um abatedouro de aves*. Master thesis, Universidade Estadual de Campinas, Campinas.

Dudley, V.E., Kolb, G.J.; Mahoney, A.R., Mancini, T.R., Matthews, C.W., Sloan, M. and Kearney, D., 1994. “Test results: SEGS LS-2 solar collector”. *Report of Sandia National Laboratories (SANDIA-94-1884)*.

Duffie, J.A. and Beckman, W.A., 2013. *Solar Engineering of Thermal Process*. John Wiley & Sons, New Jersey, 4th edition.

García-Valladares, O. and Velázquez, N., 2009. “Numerical simulation of parabolic trough solar collector: Improvement using counter flow concentric circular heat exchangers”. *International Journal of Heat and Mass Transfer*, Vol. 52, p. 597-609.

Ghisi, E., Gosch, S. and Lamberts, R., 2007. “Electricity end-uses in the residential sector of Brazil”. *Energy Policy*, Vol. 35, n. 8, p. 4107-4120.

Herold, K.E., Radermacher, R. and KLEIN, S.A., 1996. *Absorption chillers and heat pumps*. Crc Press, Boca Raton.

Incropera, F.P., Dewitt, D.P., Bergman, T. L., Lavine, A.S., 2008. *Fundamentos de transferência de calor e massa*. LTC, Rio de Janeiro.

Kim, D.S. and Ferreira, C.A.I., 2008. “Solar refrigeration options – a state-of-the-art review”. *International journal of refrigeration*, Vol. 31, p .3–15.

Kreith, F. and Bohn, M.S., 2003. *Princípios de transferência de calor*. Thomson, São Paulo.

Loikits Distribution LTD., "Syltherm 800 technical data sheet". 3 Out. 2017 <http://www.loikitsdistribution.com/files/syltherm-800-technical-data-sheet.pdf>.

Marc, O., Sinama, F.; Praene, J.P., Lucas, F. and Castaing-Lasvignottes, J., 2015. "Dynamic modeling and experimental validation elements of a 30 kW LiBr/H2O single effect absorption chiller for solar application". *Applied Thermal Engineering*, Vol. 90, p. 980-993.

Munhoz, F.C. and Garcia, A., 2008. "Caracterização da velocidade e direção predominante dos ventos para a localidade de Ituverava-SP". *Revista Brasileira de Meteorologia*, Vol. 23, n. 1, p. 30-24.

Patankar, S.V., 1980. *Numerical Heat Transfer and Fluid Flow*. McGraw-Hill Book Company, New York.

Sarbu, I. and Sebarchievici, C., 2015 "General review of solar-powered closed sorption refrigeration systems". *Energy Conversion and Management*, Vol. 105, p. 403-422.

Sintali, I.S., Egbo, G. and Dandakouta, H., 2014, "Energy equations for computation parabolic-trough collector efficiency using solar position coordinates". *American Journal of Engineering Research*, Vol. 3, n. 10, p. 25-33.

SWERA, "Solar and Wind Energy Resource Assessment". 15 Feb. 2017 <https://maps.nrel.gov/swera/>.

Tzivandis, C., Bellos, E., Korres, D., Antonopoulos, K.A.; Mitsopoulos, G., 2015. "Thermal and optical efficiency investigation of a parabolic trough collector". *Case Studies in Thermal Engineering*, Vol. 6, p. 226-237.

Weather Spark. 18 Out. 2017 <https://pt.weatherspark.com/>.

Zarza Moya, E. and Ciemat., 2012. "Parabolic-trough concentrating solar power (CSP) systems". Published in K. Lovegrove and W. Stein (Eds.), *Concentrating solar power technology: Principles, developments and applications*. Woodhead Publishing Series in Energy, Cambridge , n. 21, chap. 2, p. 197-239.

7. RESPONSIBILITY NOTICE

The authors are the only responsible for the printed material included in this paper.